Hindawi
Journal of Nanomaterials
Volume 2020, Article ID 7029601, 12 pages
https://doi.org/10.1155/2020/7029601

Research Article

Green Synthesis of Graphene from Graphite in Molten Salt Medium

Betül Gürünlü, Çiğdem Taşdelen Yücedağ, and Mahmut Rahim Bayramoğlu

Chemical Engineering Department, Gebze Technical University, Cayırova Campus, Gebze, Kocaeli, Turkey

Correspondence should be addressed to Betül Gürünlü; betulgurunlu@gmail.com

Received 10 September 2019; Revised 19 December 2019; Accepted 28 December 2019; Published 31 January 2020

Academic Editor: Paul Munroe

Green synthesis of graphene from graphite was carried out in molten salt mixture of LiCl-KCl, which is an environmentally friendly alternative to traditional methods using a large number of chemicals. The effect of carbonization temperature on the final properties of graphene products was investigated at a temperature range of 500-800°C. The layer numbers of graphene products were determined as a single layer and few layers by XRD and Raman analyses. The highest conductivity value of 1219 S/m was reached with the sample synthesized at 600°C (GGr600), which is 10-fold higher than that of commercial graphene (CG) (115 S/m). The percentage of carbon contents of GGr600 and sample synthesized at 800°C (GGr800) was determined as 86% and 73% by XPS. From the SEM analyses, it was observed that graphene products have sheet-like structures. A TEM image showed that GGr800 has the thickness changing from 5-9 nm, pointing out the graphene with few layers. AFM analysis demonstrated that GGr600 has a single-layer sheet-like structure.

1. Introduction

Graphene, which is a quasi-two-dimensional carbon, has become a very popular material in recent years with a wide range of applications [1]. Graphene is a single atomic layer of graphite with a 0.34 nm thickness, first discovered by Geim and Novoselov in 2004 [2–4]. It is a sheet of sp^2-bound carbon atoms organized into a hexagonal lattice [5, 6]. Graphene has many superior physical and chemical properties such as mechanical strength, thermal conductivity, high mobility, optical transparency, and room temperature quantum Hall effect and excellent electronic properties such as Dirac particles with linear dispersion, transport energy gap, and simply absorption coefficient of lights [7, 8]. In particular, due to its high electrical conductivity, it has many applications such as fuel cells, solar cells, anticorrosive materials, circuit boards, OLED display panels, longer-lasting batteries, and supercapacitors [9–11].

Graphene synthesis methods are divided into two categories such as top-down and bottom-up approaches [12, 13]. In the top-down process, graphitic microstructures such as graphite, carbon fibers, and carbon nanotubes are the starting materials and individual graphene layers are extracted or peeled either by physical, electrochemical, or chemical methods such as the chemical reduction of graphite oxide, among which Hummer's method is the most popular [14–16]. The bottom-up approach implements carbon atoms as building blocks; epitaxial growth of graphite on SiC surfaces and chemical vapor deposition are the most sophisticated methods [17]. Further, various inexpensive and simple molecules such as naphthalene, benzene, hexane, alfalfa plant, glucose, and cellulose can be utilized as a starting material in this approach [18–22].

Furthermore, various popular techniques such as Hummers' method, liquid-phase exfoliation of graphite, and chemical vapor deposition suffer from disadvantages such as low quality of the graphene product, low rate of production, and use of hazardous chemicals [23, 24]. Most of the chemical methods, which have been used up to now, include harsh oxidizers such as $H_2SO_4/KMnO_4$ or carboxylic acid, formic acid, and organic solvents, all of which are environmentally detrimental [25, 26]. The electrochemical exfoliation of graphite into graphene sheets via molten salts is a promising alternative method, which decreases the number

of defects in the graphene structure in comparison to traditional chemical-rich methods [27, 28]. The molten salt process is based on the interaction of alkali ions with graphite that enables the formation of graphene nanosheets and flakes [29].

The eco-friendly production of graphene by the electrochemical exfoliation of graphite in molten LiCl (Green Chemistry 18 (2016), 1952-1964), molten NaCl (Journal of Industrial and Engineering Chemistry 52 (2017), 18-27), and molten LiCl-NaCl (Applied Surface Science 490 (2019), 383-394) has been demonstrated [30–32]. Also, the chemical exfoliation of graphite powder in molten LiCl was reported. The molten salt approach has several advantages such as simplicity, high productivity, low cost, and short processing times compared to other methods used for the production of graphene. In this study, the eco-friendly synthesis of graphene in the eutectic salt mixture of LiCl/KCl is reported. It was shown that graphite can be converted into nanostructured carbons in an ionic molten salt (MS) medium, and the process yields purer graphene via tuning of the synthesis conditions. Therefore, a series of experiments at different temperatures were conducted to investigate the effect of temperature on the product quality.

2. Materials and Methods

2.1. Materials. As commercial graphite (CGr), natural flake graphite, grade 3061, was purchased from Asbury Graphite Mills, Inc., New Jersey. Commercial graphene (CG) was obtained from XG Sciences, Michigan, US. Other chemicals used in the experiments were of analytical grade: lithium chloride (Merck), potassium chloride (Riedel-de Haen), sulphuric acid (95-97%, Merck), potassium permanganate (Merck), sodium hydroxide (Sigma-Aldrich), L-ascorbic acid (Carlo Erba), and hydrochloric acid (37%, J.T.Baker).

2.2. Experimental System and Synthesis Method. Graphene was synthesized by heating the graphite under flowing argon or nitrogen atmosphere in a stainless steel reactor surrounded by a ceramic heater. The experimental system is shown in Figure 1. The temperature of the system was controlled by an Elimko E-200 Series digital temperature controller. The graphite was mixed with the eutectic composition of LiCl/KCl (45/55 by weight) with a ratio (1 : 10), and the powders were homogenized by pestling into an agate mortar. The mixture was then filled into a ceramic crucible and loaded into the reactor. First, the system was vacuumed and then flushed with the reaction gas (Ar or N_2) for 5 min. After the starting step, the system was heated to the desired temperature with a 20°C min^{-1} heating rate and kept at this temperature for 5 h. Finally, the system was cooled to room temperature by turning off the power; meanwhile, the gas flow was fed until the temperature fell below 50°C. The acquired block of products was crushed into particles and washed with a sufficient amount of water to remove the salts. The synthesized material was dried overnight in a drying oven at 60°C.

For comparison, reduced graphene oxide (RGO) was synthesized by modified Hummer's method; 1 g of graphite was added to 50 mL concentrated sulphuric acid while stirring in an ice water bath. Then, 3 g potassium permanganate was slowly added by controlling the temperature under 55°C. After that, the suspension was stirred at 25°C for 25 min followed by 5 min sonication in an ultrasonic bath (Elmasonic S, 30H). After repeating the stirring-sonication step 12 times, the reaction was cooled by the addition of 200 mL distilled water. An extra 2 h ultrasonic treatment was performed. After adjusting the pH to 6 by the addition of 1 M sodium hydroxide solution, the suspension was further sonicated for 1 h. 10 g L ascorbic acid was dissolved in 100 mL distilled water, and then, it was slowly added to the exfoliated graphite oxide suspension at room temperature. The reduction was performed at 95°C for 1 h. The resultant black precipitates were filtered using a cellulose filter paper and washed with 1 M hydrochloric acid solution and distilled water to neutral pH. Finally, the filtrate was dried in a drying oven to obtain the RGO powder.

2.3. Characterization of Synthesized Samples. X-ray diffraction (XRD) patterns were obtained with a Rigaku D-Max 2200 Series equipped with Cu-Kα radiation ($\lambda = 1.54$ Å) at a scanning rate of 3° per minute. The tube voltage was 40 kV, and the current was 40 mA. XPS measurements were made using a Thermo Scientific K-Alpha X-ray Photoelectron Spectrometer, which has energy range between 100 and 4000 eV, a source-defined analysis area from 30 to 400 μm, a 180° double-focusing hemispherical analyser, and a 128-channel detector.

The microstructures of the synthesized graphene were determined using a scanning electron microscope (FEI Philips XL30 SFEG SEM) and a transmission electron microscope (Hitachi HT7800 TEM operating at 120 kV). The atomic force microscope (AFM) images for the graphene samples were taken with a Veeco NanoScope IV at a contact mode.

Raman spectra were recorded in a Renishaw inVia Raman microscope using a 5x optical lens and a 532 nm laser diode with 50 mW as the excitation source. UV-vis spectral measurements were acquired using a PerkinElmer Precisely Lambda 35 UV-vis Spectrometer. An ultrasonicated suspension of the product in water was used for this analysis. The ultrasonication was performed using an ultrasonic (US) generator (Bandelin® HD 2200 SONOPULS, 200 W, 20 kHz) equipped with a horn-type probe which was used to deliver pulsed ultrasound with controllable power.

Particle sizes of the samples were measured using a Malvern Zetasizer Nano ZS Laser Particle Size Distribution Meter. Samples were dispersed in distilled water and were then agitated at 1600 rpm by using an IKA® MS 1 shaker.

Electrical conductivity tests were conducted using a Keithley 2400 SourceMeter. First, synthesized graphene samples and commercial products were placed in a cylindrical copper container, which has a copper cap. Then, graphene powders were compressed by a hydraulic press under 5 MPa for 0.5 h. The electrical resistivities of the graphene powders were determined by a four-point probe method. Pressure was applied by a joiner's clamp onto the graphene powder in the copper mold during the electrical conductivity measurement.

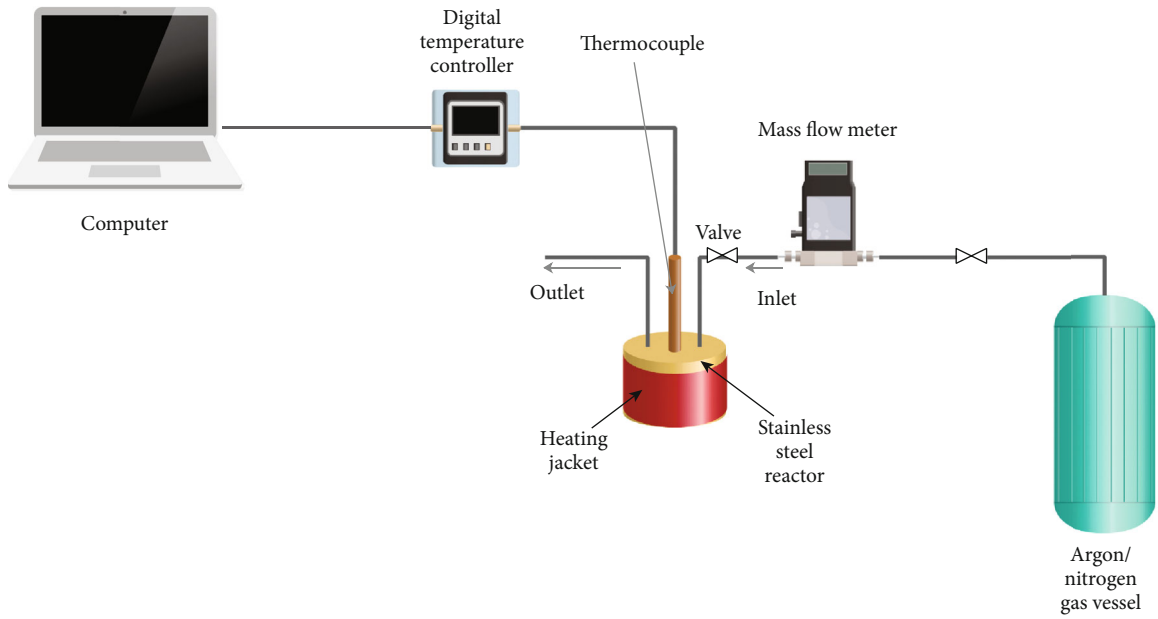

FIGURE 1: Experimental setup. Reaction was performed inside a fixed bed reactor wrapped with a ceramic heating jacket. An Ar or N_2 gas tube was connected to a mass flow meter. Inert gas was adjusted by a mass flow meter located between the gas vessel and valve. Reaction temperature was controlled by the thermocouple placed into the fixed bed into the reactor.

3. Results and Discussion

The green synthesis of graphene from graphite was conducted by using molten salt mixture LiCl/KCl at different reaction temperatures of 500°C, 600°C, 700°C, and 800°C in order to examine the effect of temperature on product quality.

XRD patterns of all synthesized graphene products as shown in Figure 2 demonstrated a peak at $2\theta = 26.5°$ which is characteristic of carbonaceous materials. Although graphene samples and CGr have the same peak position at $2\theta = 26.5°$, the peak intensities of the graphene products synthesized at 500-800°C are lower than those of CGr. This result indicates the transformation of graphite to graphene, which is in accordance with literature [33–35].

The structural analyses of graphene products were performed by using XRD. The graphene thickness can be calculated using Scherrer's equation, which is expressed by $D_{002} = K\lambda/B \cos\theta$, where D_{002} is the thickness of the crystallite (thickness of graphene), K is a constant dependent on the crystallite shape (0.89), λ is the X-ray wavelength (0.15406 nm), B is the full width at half maximum (FWHM), and θ is the scattering angle [36, 37]. The number of graphene layers was calculated by substituting the value of D_{002} obtained from Scherrer's equation into the following equation: $N_{GP} = D_{002}/d_{002}$, where d_{002} is the interlayer space for the (002) peak at $2\theta = 26.5°$ [38, 39].

As seen in Table 1, the layer number of CGr was calculated as 10, while the layer number of the CG was determined as 2. The graphene products synthesized at 500, 600, 700, and 800°C have 2, 4, 2, and 3 layers, respectively, which confirms the obtained graphene structure.

The structure of the graphene products was also evaluated by UV analyses of CG, CGr, GGr500, GGr600, GGr700, and GGr800 given in Figure 3. As seen in the spectrum, characteristic absorbance peaks at around 200 and 280 nm were observed for all samples, which is consistent with the previous studies [39–41].

Figure 4 illustrates the particle size analyses by the dynamic light scattering technique. As seen in Table 2, the particle size values of CGr, CG, GGr500, GGr600, GGr700, and GGr800 are 4180, 2402, 2660, 4205, 3017, and 3459 nm, respectively. When CGr was treated with molten salt mixture of LiCl and KCl, the particle sizes of graphene products were close to the particle size of CG. When the effect of temperature on the extent of exfoliation and reduction of GO was studied, it was observed that at higher temperatures, the crystal size of graphene became closer to that of the graphite crystal [42]. Analogously, in this study, when the reaction temperature increased, the particle diameters of graphene products became larger. On the other hand, the particle size of RGO synthesized by Hummer's method was found to be 738 nm, which agrees with the literature [43]. The reason for obtaining a smaller particle size in Hummer's method compared to the molten salt method results from the reaction steps including harsh chemicals and mechanical treatments.

The conductivity values (σ) were estimated according to $\sigma = l/AR$. In this equation, R is the electrical resistance, l is the length, and A is the cross-sectional area of the sample material. According to Table 2, the electrical conductivity values of GGr samples (GGr500, GGr600, GGr700, and GGr800) are higher than those of CG, CGr, and RGO. Hence, it can be inferred that the molten salt method has an enhancing effect on the conductivity. The increase in the conductivity is due to the advantages of the molten salt method, which enables the production of graphene with high crystallinity and purity [44]. The highest conductivity value was achieved with GGr600 at 600°C. Although the conductivity values

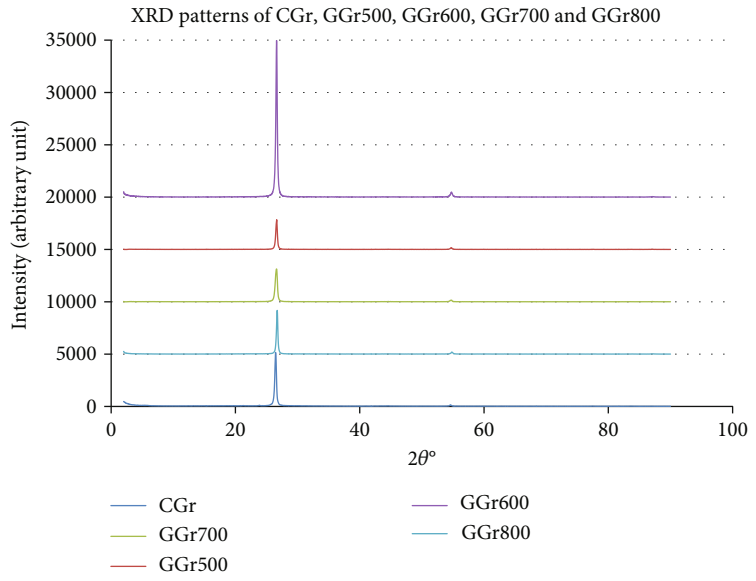

Figure 2: XRD patterns of CGr, GGr500, GGr600, GGr700, and GGr800.

Table 1: Layer numbers of synthesized graphene samples and commercial products.

Label name	Expansion	Layer numbers from XRD results
CG	Commercial graphene	2
CGr	Commercial graphite	10
RGO	Reduced graphene oxide	1
GGr500	Graphene from graphite in molten salt media at 500°C	2
GGr600	Graphene from graphite in molten salt media at 600°C	4
GGr700	Graphene from graphite in molten salt media at 700°C	2
GGr800	Graphene from graphite in molten salt media at 800°C	3

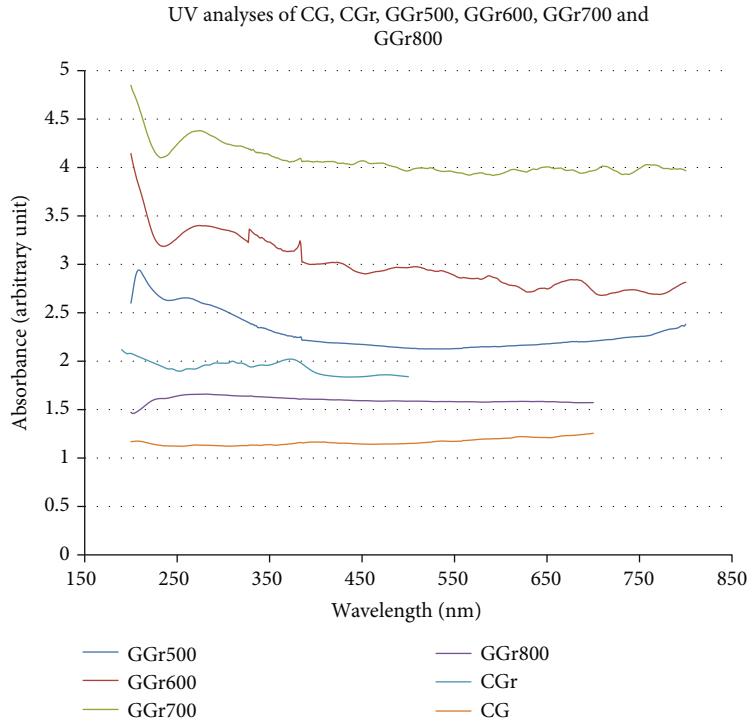

Figure 3: UV absorbance peaks of CGr, CG, and graphene products from graphite at different temperatures.

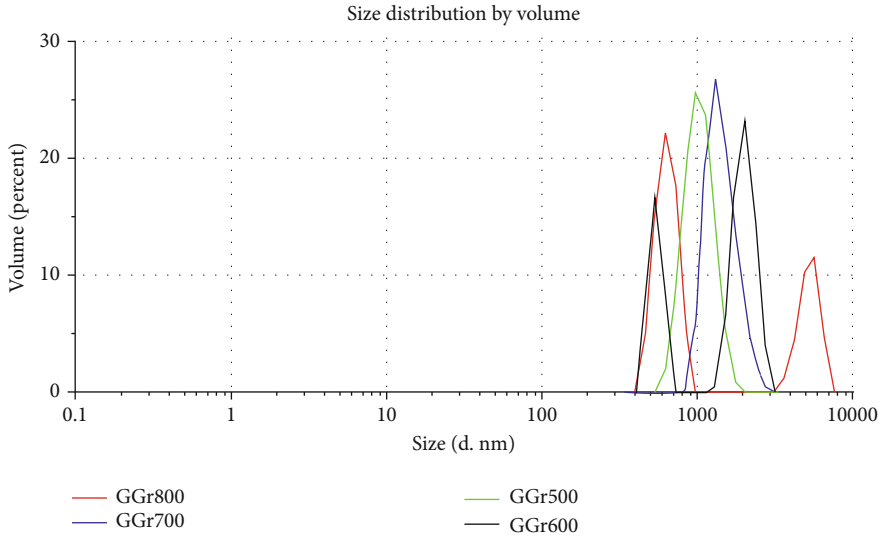

Figure 4: Particle size distribution (DLS) analyses of graphene products.

Table 2: Particle size values of synthesized graphene samples and commercial products.

Label name	Particle size (nm)	Electrical conductivities (S/m)
CG	2402	115
RGO	738	195
CGr	4180	317
GGr500	2660	1070
GGr600	4205	1219
GGr700	3017	803
GGr800	3459	724

belonging to the samples of GGr700 and GGr800 were smaller than those of the samples of GGr700 and GGr800, they are still higher than 115 S/m, which is the conductivity value of CG.

Figure 5 shows the typical Raman spectra of the CG, RGO, and GGr samples obtained at different temperatures. Characteristic graphene peaks were observed at 1345, 1576, and 2659 cm^{-1} arising from D, G, and 2D bands, respectively. For RGO, GGr500, and CG, the D band becomes stronger and broader because of the higher level of disorders of the graphene layers. GGr700 and GGr800 showed no peaks at the D band, which implies the formation of well-ordered pristine single-layer graphene without a disordered structure [45–47].

In the Raman spectra (Figure 5), the chemical change of graphite to graphene results in a notable decrease in the ID/IG ratio (Table 3). The increase in a broad 2D peak located at around 2600 cm^{-1} indicates the formation of sp^2 carbon atoms at higher heating temperatures [19, 48, 49].

In order to clarify the structure of the graphene products, the ID/IG ratios giving the information on the structural quality and order were calculated. Since the ID/IG ratio of CG is lower than 0.33, the fewer defects and functional groups were observed in the structure. In addition, synthesized GGr700 and GGr800 samples have a smaller D band, which reflects good quality and an ordered graphene structure. The most prominent features in the Raman spectra of the monolayer graphene are the G band appearing at 1582 cm^{-1} [50]. In fact, the G band is the only band from a normal first-order Raman scattering process in graphene [51]. From the G band, information such as the existence of strain, the effect of gate doping, and the impurity can be obtained about the sample. Since the peak position of the G band is sensitive to the gate voltage applied to the graphene, the Fermi energy can be evaluated by the peak position [52]. The G band arises from the stretching of the C-C bond in the graphitic materials, and it is common to all sp^2 carbon systems. The G band is highly sensitive to strain effects in the sp^2 system, and thus, it can be used to probe modification on the flat surface of graphene. Therefore, it can be understood that GGr700 has the highest G band, which indicates the high amount of sp^2 carbon content.

It is known that if the ID/IG ratio is equal to 0.6, graphene includes few layers. Moreover, when the ID/IG ratio has a value of 0.4, graphene contains a single-layer structure [53]. According to the results given in Table 3, when the higher reaction temperatures were applied in the synthesis of graphene products, the ID/IG ratios decreased. Besides, the ID/IG ratios of CG and RGO are 0.18 and 1.04, respectively. It can be concluded that GGr600, GGr700, and GGr800 have a single layer, GGr500 has few layers, and RGO has multilayers. Therefore, it may be inferred that the molten salt method applied at high temperatures results in graphene with a defect-free structure and single layer.

The presence of sp^2- and sp^3-bonded carbon atoms and the remaining functional groups were quantified by X-ray photoelectron spectroscopy (XPS; Figure 6, Table 4). The characteristic peaks of C=C, C-O-C, O-C=O, and C-C bonds are located at 284.30, 286.26, 290.34, and 285.11 eV for the

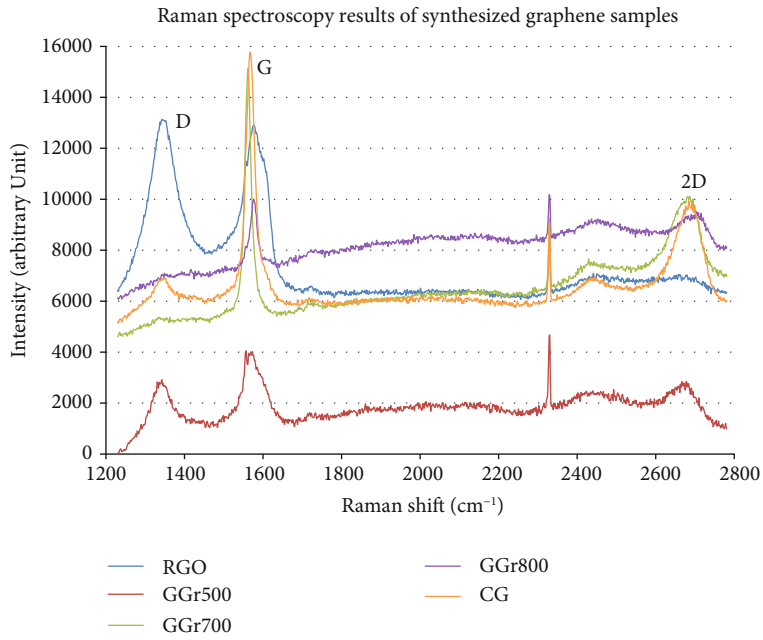

Figure 5: Raman spectra of RGO, CG, GGr500, GGr700, and GGr800.

GGr600 sample, whereas these bonds arose at 284.24, 286.28, 290.37, and 285.02 eV for the GGr800 sample, respectively. These results are compatible with the previous studies [19, 20, 42, 54].

The carbon contents of graphene products are listed in Table 4. As evident from the results, the carbon content decreases by increasing temperature. As the reaction temperature of the carbonization process increases, the carbon fraction of the graphene products generally increases [19]. However, the carbon content of GGr600 is lower than that of GGr800. The oxygen atoms, which originate from the usage of water in the purification steps, may interact with the carbon in the reaction medium. This induced an increase in the amount of functional groups in the structure of GGr800 and caused the graphitic carbon percentage to decrease.

The atomic ratios of C1s and O1s regions belonging to GGr600 and GGr800 samples are given in Table 5. The existence of oxygen content may arise from the treatments after the reaction such as washing with water to remove molten salt from the reaction mixture and storage conditions such as exposure to humid air.

The morphological structures of graphene products were examined by SEM analysis (Figure 7). SEM images of all products demonstrate sheet-like structures such as flakes, edges, and layers. From the image of the GGr600 sample, these sheet-like structures can be seen clearly in comparison to other samples. On the other hand, the SEM images of GGr500, GGr700, and GGr800 samples include the overlapping layers of graphene flakes with arbitrary shapes and random in-plane orientation [19, 20, 54].

These flakes have different sizes and shapes. Edges and intersecting lines of a flake are drawn, and the intersecting lines are used to determine the average flake size. The average

Table 3: ID/IG ratio of synthesized graphene and commercial products.

Sample name	ID/IG*
GGr500	0.74
GGr600	0.32
GGr700	0.11
GGr800	0.33
CG	0.18
RGO	1.04

*ID/IG = ratio of intensity of the D peak to G peak.

size of the flakes (L) observed in SEM images was calculated as 2 μm by using the following equation [55]:

$$L = \frac{L_{\text{Blue}} + L_{\text{Red}} + L_{\text{Yellow}}}{3}. \quad (1)$$

The sheet-like structure is further confirmed by transmission electron microscopy (TEM) imaging as seen in Figure 8. TEM images display that the graphene structure with different thickness, ranging from 5 nm to 9 nm, indicates the presence of few-layer graphene. Thicker layers are observed in significant amounts indicating that most of the graphene samples have few and multilayers. This deviation from the ideal thickness of 0.335 nm (interlayer distance in graphite along the c axis) for chemically derived single-layer graphene can be explained by the presence of a structural disorder and the remaining attached functional groups [19].

The AFM characterization of the final graphene products (GGr500, GGr600, GGr700, and GGr800) was performed to measure the surface roughness and thickness to determine the optimal temperature for graphene growth. Roughness

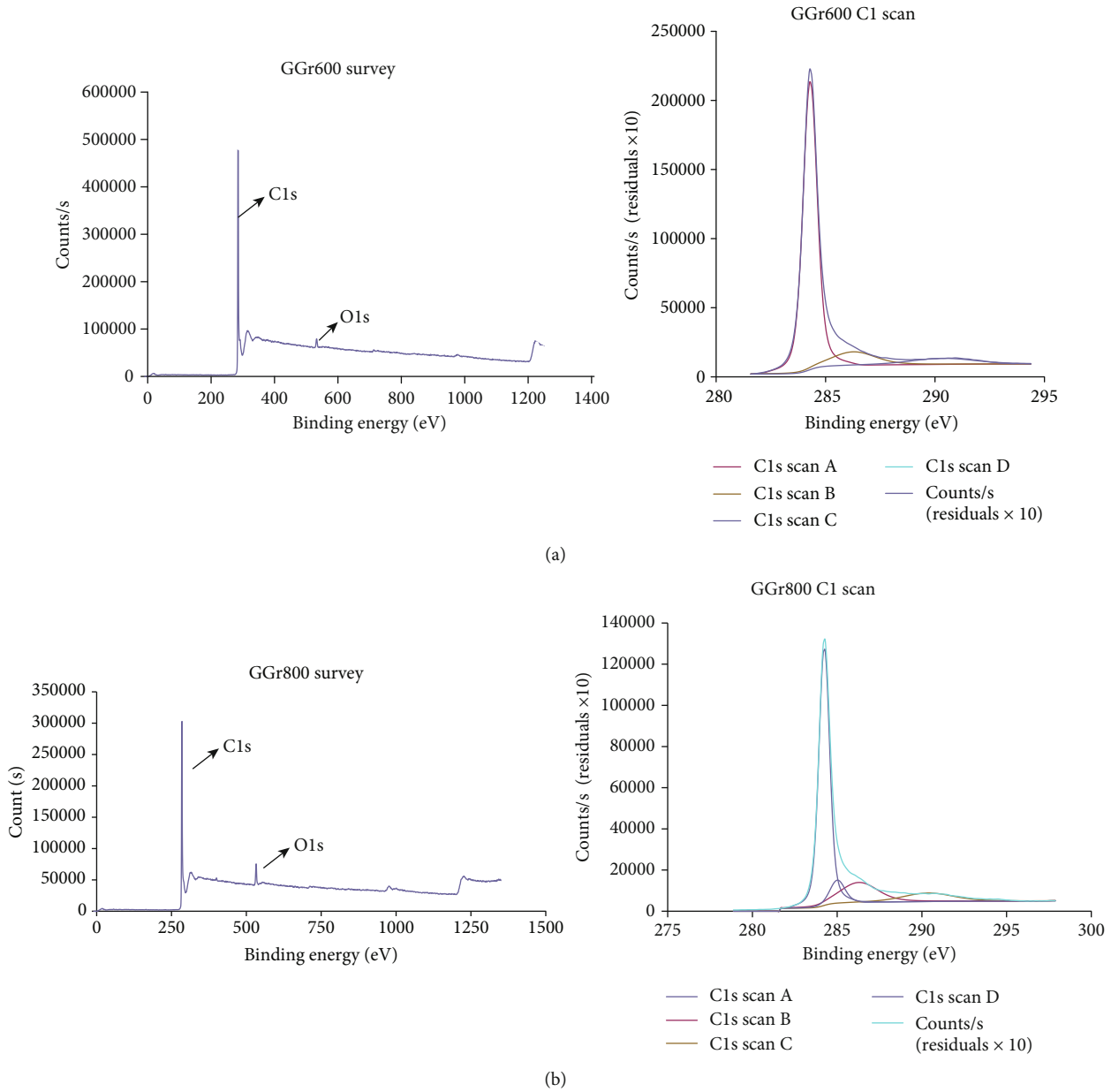

Figure 6: Survey-scanned XPS spectra and fine-scanned spectra of (a) GGr600 and (b) GGr800.

Table 4: Contribution from differently bonded carbons extracted through peak deconvolution for the C1s region for GGr600 and GGr800.

Bond structure	GGr600		GGr800	
	Binding energy peaks (eV)	Atomic %	Binding energy peaks (eV)	Atomic %
C=C	284.30	79.86	284.24	64.56
C-O-C	286.26	10.93	286.28	17.53
O-C=O	290.34	7.13	290.37	9.82
C-C	285.11	7. 08	285.02	8.09

Table 5: C1s and O1s regions' atomic ratio values and peak for GGr600 and GGr800.

	GGr600		GGr800	
	Peak binding energy (eV)	Atomic %	Peak binding energy (eV)	Atomic %
C1s	284.8	97.9	284.8	93.81
O1s	532.02	2.1	532.65	5.45
N1s	n/a	n/a	400.26	0.74

average (Ra), calculated by measuring height alterations on the surface, is less sensitive to big peaks and valleys. The root mean square roughness (Rq) value is the square root of the total of the squares of the particular vertical deviations from the average level [1]. The roughness mean square (RMS) value, which gives the average height deflections of the average level, is estimated by measuring the heights of surfaces of microscopic peaks and valleys. The number of graphene

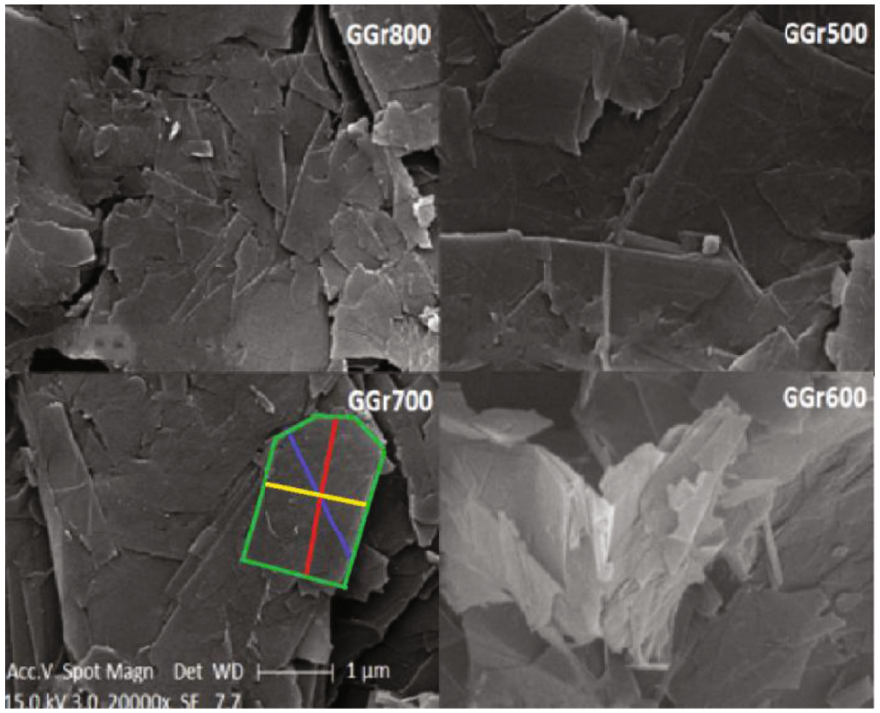

Figure 7: SEM images of graphene products.

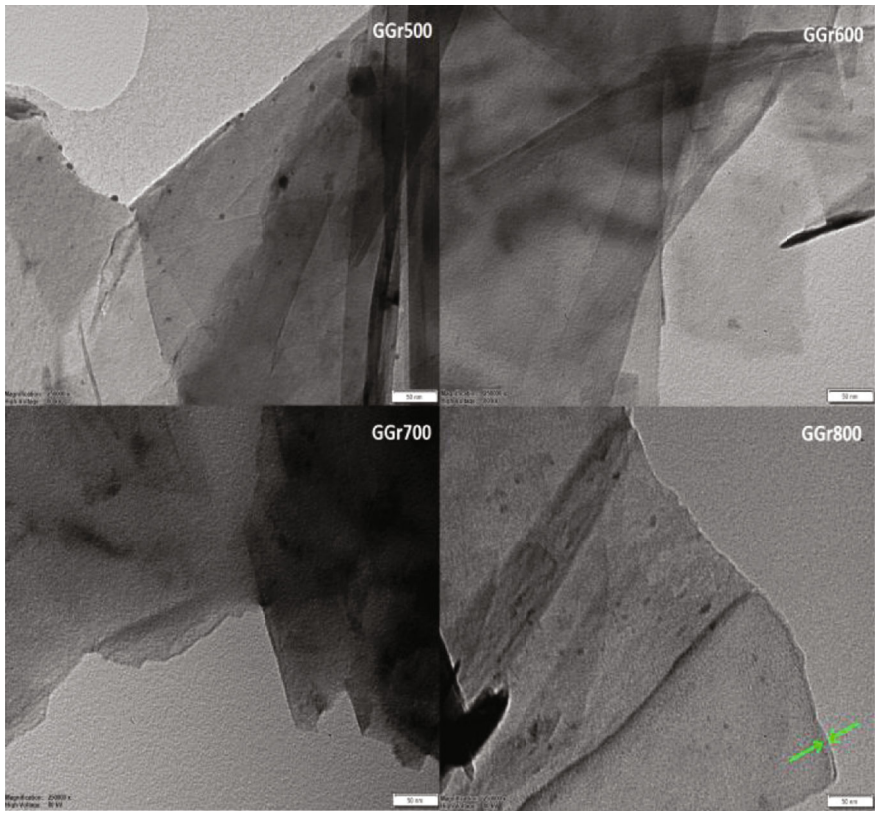

Figure 8: TEM images of graphene products.

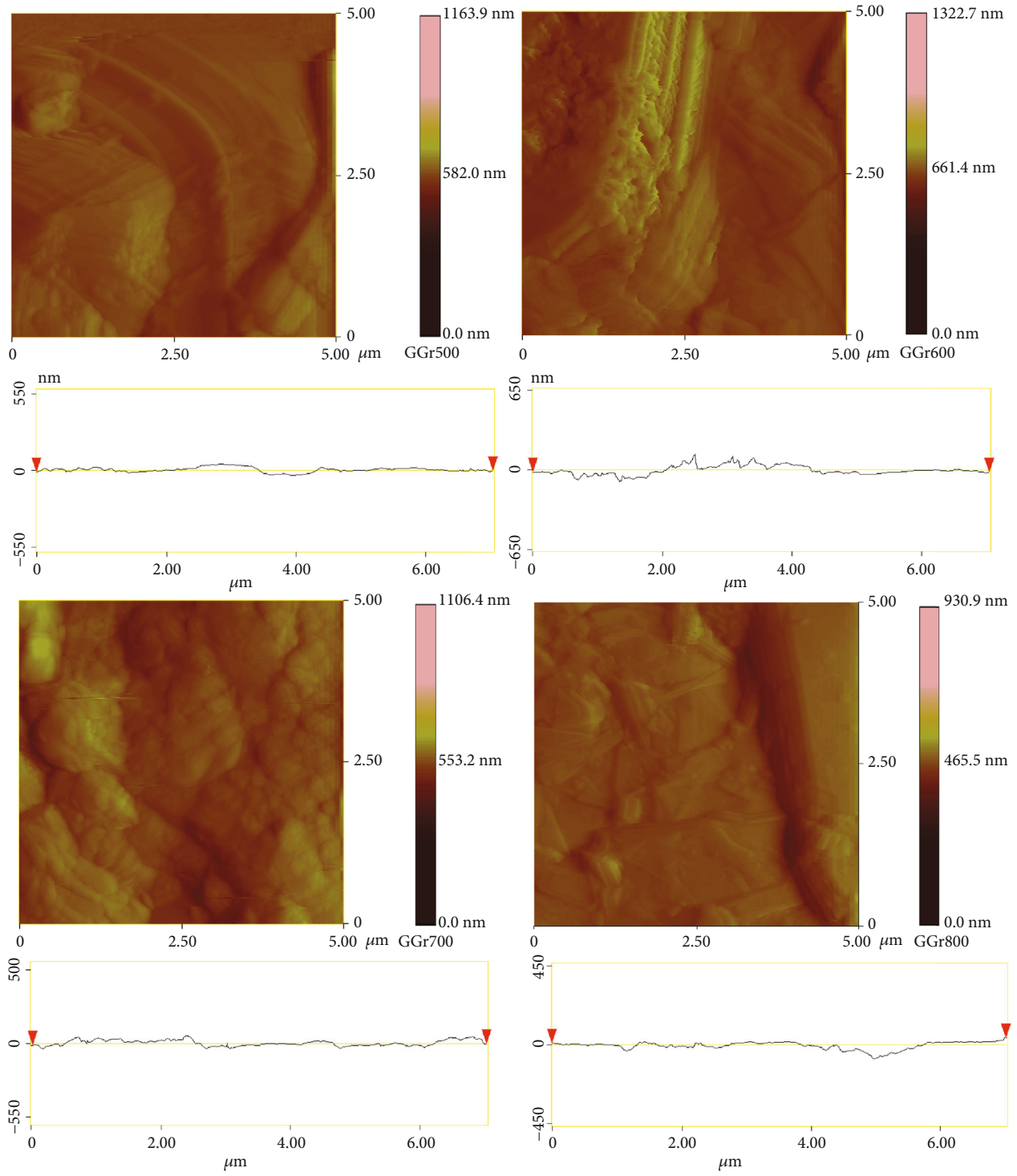

Figure 9: AFM images and line profiles of graphene samples.

layers, N, is calculated via AFM by the following equation assuming the value of single-layer graphene (SLG) thickness as 0.335 nm:

$$N = (t_{\text{measured}} - 0.4)/0.335, \quad (2)$$

where t_{measured} is the thickness determined by AFM to exclude the increase in thickness contributed by the substrate-graphene and graphene-tip interactions. The value of 0.4 is the arbitrary magnitude (equivalent to three graphene layers with 0.335 nm spacing). N can be calculated via AFM by measuring the height of the deposited graphene flakes [56]. The height of SLG is strongly affected by the structure. For example, when SiO_2 and mica are chosen as substrates, the heights of SLG are ~1 nm and 0.4 nm, respectively [57].

The AFM characterization results of samples (GGr500, GGr600, GGr700, and GGr800) are summarized in Figure 9. The Ra values of GGr500, GGr600, GGr700, and GGr800 are 13.052, 30.110, 17.431, and 16.982 nm, respectively.

The Rq values of GGr500, GGr600, GGr700, and GGr800 are 21.969, 36.234, 33.244, and 24.348 nm, respectively. The RMS values of GGr500, GGr600, GGr700, and GGr800 are 17.491, 38.027, 20.404, and 22.120 nm, respectively. Vertical distance denotes the thickness of graphene, and it is determined for GGr500, GGr600, GGr700, and GGr800 to be 7.298, 1.500, 7.406, and 27.695 nm, respectively. As the temperature increases, the thickness of the graphene products increases as well. The layer numbers were calculated via Equation (2). The layer numbers of GGr500, GGr600, GGr700, and GGr800 are 21, 3, 21, and 81, respectively. According to AFM results, the best results are obtained at 600°C temperature.

4. Conclusions

In this study, graphene was synthesized from graphite via the molten salt method. The synthesized graphene products were characterized by using XRD, UV-vis spectroscopy, DLS, electrical conductivity measurements, XPS, Raman spectroscopy, TEM, SEM, and AFM.

From the XRD results, all synthesized graphene products showed a $2\theta = 26.5^{\circ}$ peak that is characteristic of graphene and most of the synthesized graphene samples include 3 layers in average. These results are supported with the layer numbers that are obtained from Raman results; the ID/IG results show that most of the graphene products are few-layered. The UV-vis spectrum of GGr500, GGr600, GGr700, and GGr800 shows a peak around at 275-285 nm revealing the graphene structure.

According to the DLS results, the particle sizes of the graphene samples increased with increasing temperature. The electrical conductivities of GGr samples are 7-10 times higher than the electrical conductivity of CG. The XPS spectrum of GGr600 and GGr800 contains four peaks at ~284, 286, 290, and 285 eV, which correspond to the C=C, C-O-C, O-C=O, and C-C bonds, respectively. From the XPS results, it can be concluded that the carbon content of GGr decreases with increasing temperature. The Raman spectra consist of D, G, and 2D bands located at 1345, 1576, and 2659 cm^{-1}, respectively. The synthesized GGr700 and GGr800 samples have a lower D band indicating that the ordered graphene structure included fewer defects and had good quality. According to ID/IG values, GGr600, GGr700, and GGr800 have a single layer, GGr500 has few layers, and RGO has multilayers. Graphene morphology was confirmed via both SEM and TEM studies. The average size of flakes observed in the SEM images was calculated as 2 μm. The TEM images show graphene structures with different thicknesses, ranging from 5 nm to 9 nm, indicating the presence of few-layer graphene. The layer numbers of GGr500, GGr600, GGr700, and GGr800 were calculated via AFM results as 21, 3, 21, and 81, respectively. Thus, it can be concluded that lower temperature gives better results.

Data Availability

The data used to support the findings of this study are included within the article.

Conflicts of Interest

The authors declare that there is no conflict of interest regarding the publication of this paper.

Acknowledgments

This work was supported by Gebze Technical University (GTU). The authors thank the Materials Science and Engineering Department of GTU for providing XRD measurements and particle size analyses and Advanced Technologies R&D Center of Bogazici University (BOUN) for XPS and Raman measurements. We would like to thank Editage (https://www.editage.com) for English language editing. Also, very special thanks are due to Bermak Kalip for lathe operations.

References

[1] W. Choi and J.-W. Lee, *Graphene: Synthesis and Applications*, CRC Press, Taylor and Francis Group, 1st edition, 2011.

[2] F. Schwierz, "The rise and rise of graphene," *Nature Nanotechnology*, vol. 5, no. 11, p. 755, 2010.

[3] A. K. Geim, "Graphene: status and prospects," *Science*, vol. 324, no. 5934, pp. 1530–1534, 2009.

[4] A. K. Geim and K. S. Novoselov, "The rise of graphene," in *Nanoscience and Technology*, pp. 11–19, Nature Publishing Group, 2009.

[5] M. J. Allen, V. C. Tung, and R. B. Kaner, "Honeycomb carbon: a review of graphene," *Chemical Reviews*, vol. 110, no. 1, pp. 132–145, 2010.

[6] J. C. Meyer, A. K. Geim, M. I. Katsnelson, K. S. Novoselov, T. J. Booth, and S. Roth, "The structure of suspended graphene sheets," *Nature*, vol. 446, no. 7131, pp. 60–63, 2007.

[7] S. Bharech and R. Kumar, "A review on the properties and applications of graphene," *Journal of Material Science and Mechanical Engineering*, vol. 2, no. 10, pp. 70–73, 2015.

[8] Y. Zhu, S. Murali, W. Cai et al., "Graphene and graphene oxide: synthesis, properties, and applications," *Advanced Materials*, vol. 22, no. 35, pp. 3906–3924, 2010.

[9] E. P. Randviir, D. A. C. Brownson, and C. E. Banks, "A decade of graphene research: production, applications and outlook," *Materials Today*, vol. 17, no. 9, pp. 426–432, 2014.

[10] A. H. Castro Neto, F. Guinea, N. M. R. Peres, K. S. Novoselov, and A. K. Geim, "The electronic properties of graphene," *Reviews of Modern Physics*, vol. 81, no. 1, pp. 109–162, 2009.

[11] P. Avouris, "Graphene: electronic and photonic properties and devices," *Nano Letters*, vol. 10, no. 11, pp. 4285–4294, 2010.

[12] V. Sridhar, J. H. Jeon, and I. K. Oh, "Synthesis of graphene nano-sheets using eco-friendly chemicals and microwave radiation," *Carbon*, vol. 48, no. 10, pp. 2953–2957, 2010.

[13] R. S. Edwards and K. S. Coleman, "Graphene synthesis: relationship to applications," *Nanoscale*, vol. 5, no. 1, pp. 38–51, 2013.

[14] S. Park and R. S. Ruoff, "Chemical methods for the production of graphenes," *Nature Nanotechnology*, vol. 4, no. 4, pp. 217–224, 2009.

[15] S. Stankovich, D. A. Dikin, R. D. Piner et al., "Synthesis of graphene-based nanosheets via chemical reduction of exfoliated graphite oxide," *Carbon*, vol. 45, no. 7, pp. 1558–1565, 2007.

[16] L. Jiao, L. Zhang, X. Wang, G. Diankov, and H. Dai, "Narrow graphene nanoribbons from carbon nanotubes," *Nature*, vol. 458, no. 7240, pp. 877–880, 2009.

[17] L. G. de Arco, Yi Zhang, A. Kumar, and Chongwu Zhou, "Synthesis, transfer, and devices of single- and few-layer graphene by chemical vapor deposition," *IEEE Transactions on Nanotechnology*, vol. 8, no. 2, pp. 135–138, 2009.

[18] L. Zhi and K. Mullen, "A bottom-up approach from molecular nanographenes to unconventional carbon materials," *Journal of Materials Chemistry*, vol. 18, no. 13, pp. 1472–1484, 2008.

[19] X. Liu, C. Giordano, and M. Antonietti, "A facile molten-salt route to graphene synthesis," *Small*, vol. 10, no. 1, pp. 193–200, 2014.

[20] B. Gurunlu and M. Bayramoglu, "One step synthesis of graphene-like structures by carbonization of some carbohydrates in molten salt media," *Journal of Nano Research*, vol. 59, pp. 166–179, 2019.

[21] J. Qu, C. Luo, Q. Zhang, Q. Cong, and X. Yuan, "Easy synthesis of graphene sheets from alfalfa plants by treatment of nitric acid," *Materials Science and Engineering: B*, vol. 178, no. 6, pp. 380–382, 2013.

[22] A. S. Kolesnikova, R. A. Safonov, O. A. Shinkarenko, A. S. Chumakov, E. M. Soldatenko, and E. G. Glukhovskoy, "Synthesis of graphene from naphthalene molecules on the surface of a Langmuir monolayer," *Journal of Surface Investigation: X-ray, Synchrotron and Neutron Techniques*, vol. 11, no. 3, pp. 510–516, 2017.

[23] A. R. Kamali, J. Feighan, and D. J. Fray, "Towards large scale preparation of graphene in molten salts and its use in the fabrication of highly toughened alumina ceramics," *Faraday Discussions*, vol. 190, pp. 451–470, 2016.

[24] A. Ibarra-Hernández, A. Vega-Rios, and V. Osuna, "Synthesis of graphite oxide with different surface oxygen contents assisted microwave radiation," *Nanomaterials*, vol. 8, no. 2, p. 106, 2018.

[25] J. Li, X. Zeng, T. Ren, and E. van der Heide, "The preparation of graphene oxide and its derivatives and their application in bio-tribological systems," *Lubricants*, vol. 2, no. 3, pp. 137–161, 2014.

[26] M. Mitra, K. Chatterjee, K. Kargupta, S. Ganguly, and D. Banerjee, "Reduction of graphene oxide through a green and metal-free approach using formic acid," *Diamond and Related Materials*, vol. 37, pp. 74–79, 2013.

[27] H. Huang, Y. Xia, X. Tao et al., "Highly efficient electrolytic exfoliation of graphite into graphene sheets based on Li ions intercalation–expansion–microexplosion mechanism," *Journal of Materials Chemistry*, vol. 22, no. 21, pp. 10452–10456, 2012.

[28] H. K. Kim, A. R. Kamali, K. C. Roh, K. B. Kim, and D. J. Fray, "Dual coexisting interconnected graphene nanostructures for high performance supercapacitor applications," *Energy & Environmental Science*, vol. 9, no. 7, pp. 2249–2256, 2016.

[29] A. R. Kamali and D. J. Fray, "Large-scale preparation of graphene by high temperature insertion of hydrogen into graphite," *Nanoscale*, vol. 7, no. 26, pp. 11310–11320, 2015.

[30] A. R. Kamali, "Eco-friendly production of high quality low cost graphene and its application in lithium ion batteries," *Green Chemistry*, vol. 18, no. 7, pp. 1952–1964, 2016.

[31] A. R. Kamali, "Scalable fabrication of highly conductive 3D graphene by electrochemical exfoliation of graphite in molten NaCl under Ar/H_2 atmosphere," *Journal of Industrial and Engineering Chemistry*, vol. 52, pp. 18–27, 2017.

[32] L. Labiadh and A. R. Kamali, "3D graphene nanoedges as efficient dye adsorbents with ultra-high thermal regeneration performance," *Applied Surface Science*, vol. 490, pp. 383–394, 2019.

[33] W. Wu and H. Huang, "Derived from poplar leaves graphene-modified silicone rubber composites," *Journal of Thermoplastic Composite Materials*, 2019.

[34] D. Zhang, K. Zhang, Y. Yao et al., "Intercalation and exfoliation syntheses of high specific surface area graphene and FeC_2O_4/graphene composite for anode material of lithium ion battery," *Fullerenes, Nanotubes, and Carbon Nanostructures*, vol. 27, no. 9, pp. 746–754, 2019.

[35] W. Wang, Y. Wang, Y. Gao, and Y. Zhao, "Control of number of graphene layers using ultrasound in supercritical CO_2 and their application in lithium-ion batteries," *The Journal of Supercritical Fluids*, vol. 85, pp. 95–101, 2014.

[36] F. Su, X. S. Zhao, Y. Wang, L. Wang, and J. Y. Lee, "Hollow carbon spheres with a controllable shell structure," *Journal of Materials Chemistry*, vol. 16, no. 45, pp. 4413–4419, 2006.

[37] M. Adel, A. el-Maghraby, O. el-Shazly, E. W. F. el-Wahidy, and M. A. A. Mohamed, "Synthesis of few-layer graphene-like nanosheets from glucose: new facile approach for graphene-like nanosheets large-scale production," *Journal of Materials Research*, vol. 31, no. 4, pp. 455–467, 2016.

[38] H. M. Ju, S. H. Huh, S. H. Choi, and H. L. Lee, "Structures of thermally and chemically reduced graphene," *Materials Letters*, vol. 64, no. 3, pp. 357–360, 2010.

[39] S. Uran, A. Alhani, and C. Silva, "Study of ultraviolet-visible light absorbance of exfoliated graphite forms," *AIP Advances*, vol. 7, no. 3, article 035323, 2017.

[40] S. Wang, C. Wang, and X. Ji, "Towards understanding the salt-intercalation exfoliation of graphite into graphene," *RSC Advances*, vol. 7, no. 82, pp. 52252–52260, 2017.

[41] F. T. Thema, M. J. Moloto, E. D. Dikio et al., "Synthesis and characterization of graphene thin films by chemical reduction of exfoliated and intercalated graphite oxide," *Journal of Chemistry*, vol. 2013, Article ID 150536, 6 pages, 2013.

[42] F. T. Johra, J. W. Lee, and W. G. Jung, "Facile and safe graphene preparation on solution based platform," *Journal of Industrial and Engineering Chemistry*, vol. 20, no. 5, pp. 2883–2887, 2014.

[43] S. N. Alam, N. Sharma, and L. Kumar, "Synthesis of graphene oxide (GO) by modified Hummers method and its thermal reduction to obtain reduced graphene oxide (rGO)," *Graphene*, vol. 6, no. 1, pp. 1–18, 2017.

[44] A. Rezaei, B. Kamali, and A. R. Kamali, "Correlation between morphological, structural and electrical properties of graphite and exfoliated graphene nanostructures," *Measurement*, vol. 150, article 107087, 2020.

[45] C. Botas, P. Álvarez, C. Blanco et al., "Critical temperatures in the synthesis of graphene-like materials by thermal exfoliation–reduction of graphite oxide," *Carbon*, vol. 52, pp. 476–485, 2013.

[46] M. S. Dresselhaus, A. Jorio, M. Hofmann, G. Dresselhaus, and R. Saito, "Perspectives on carbon nanotubes and graphene

Raman spectroscopy," *Nano Letters*, vol. 10, no. 3, pp. 751–758, 2010.

[47] A. C. Ferrari and J. Robertson, "Interpretation of Raman spectra of disordered and amorphous carbon," *Physical Review B*, vol. 61, no. 20, pp. 14095–14107, 2000.

[48] A. C. Ferrari, "Raman spectroscopy of graphene and graphite: disorder, electron–phonon coupling, doping and nonadiabatic effects," *Solid State Communications*, vol. 143, no. 1-2, pp. 47–57, 2007.

[49] A. C. Ferrari, J. C. Meyer, V. Scardaci et al., "Raman spectrum of graphene and graphene layers," *Physical Review Letters*, vol. 97, no. 18, pp. 187401–187404, 2006.

[50] L. M. Malard, M. A. Pimenta, G. Dresselhaus, and M. S. Dresselhaus, "Raman spectroscopy in graphene," *Physics Reports*, vol. 473, no. 5-6, pp. 51–87, 2009.

[51] A. Jorio, M. S. Dresselhaus, R. Saito, and G. Dresselhaus, *Raman Spectroscopy in Graphene Related Systems*, John Wiley & Sons, Singapore, 2011.

[52] R. Saito, K. Sato, P. T. Araujo, D. L. Mafra, and M. S. Dresselhaus, "Gate modulated Raman spectroscopy of graphene and carbon nanotubes," *Solid State Communications*, vol. 175-176, pp. 18–34, 2013.

[53] B. Galindo, S. G. Alcolea, J. Gómez et al., "Effect of the number of layers of graphene on the electrical properties of TPU polymers," *IOP Conference Series: Materials Science and Engineering*, vol. 64, article 012008, 2014.

[54] G. Gao, D. Liu, S. Tang et al., "Heat-initiated chemical functionalization of graphene," *Scientific Reports*, vol. 6, no. 1, article 20034, 2016.

[55] H. Malekpour, K.-H. Chang, J.-C. Chen et al., "Thermal conductivity of graphene laminate," *Nano Letters*, vol. 14, no. 9, pp. 5155–5161, 2014.

[56] C. J. Shearer, A. D. Slattery, A. J. Stapleton, J. G. Shapter, and C. T. Gibson, "Accurate thickness measurement of graphene," *Nanotechnology*, vol. 27, no. 12, article 125704, 2016.

[57] A. C. Ferrari, F. Bonaccorso, V. Fal'ko et al., "Science and technology roadmap for graphene, related two-dimensional crystals, and hybrid systems," *Nanoscale*, vol. 7, no. 11, pp. 4598–4810, 2015.